applied optics

Simulation and observation for volume emission rates emitted from O_2(0-1) and O(^{1}S) nightglow in Northwest China

YUANHE TANG,[1,*] PENG SUN,[1] HAIYANG GAO,[2] JIN CUI,[1] ZIJIAN LI,[1] HAOXUAN WANG,[1] HUAN LV,[1] MIN JIA,[1] HANCHEN LIU,[3] CUNXIA LI,[1] AND QINGSONG LIU[4]

[1]School of Science, Xi'an University of Technology, Xi'an 710048, China
[2]Key Laboratory for Aerosol-Cloud-Precipitation of China Meteorological Administration, Nanjing University of Information Science and Technology, Nanjing 210044 China
[3]School of Science, Xi'an Polytechnic University, Xi'an 710048, China
[4]Key Laboratory of Spectral Imaging Technique, Xi'an Institute of Optics and Precision Mechanics, Chinese Academy of Sciences, Xi'an 710119, China
*Corresponding author: ltp1801@163.com

Received 6 November 2018; revised 18 December 2018; accepted 19 December 2018; posted 20 December 2018 (Doc. ID 351182); published 0 MONTH 0000

Being susceptible to the change of atmospheric conditions, the volume emission rate (VER) is very suitable to be used as a light source by passive remote sensing for measuring atmospheric wind and temperature. Thus, the VERs emitted from O_2(0-1) and O(^{1}S) of the nightglow at 80–120 km are studied in this paper. Based on the Naval Research Laboratory Mass Spectrometer Incoherent Scatter (NRLMSISE-00) model data and the ground-based airglow imaging interferometer (GBAII) instrument observation for a local time and place, simulated VER profiles represented by four layers are obtained for the nightglow of O_2(0-1) and O(^{1}S). The O_2(0-1) nightglow model peak values at 94 km on 6 December 6 2013 and 8 November 2011 are 8111 photons $\cdot$ cm^{-3} $\cdot$ s^{-1} and 8406 photons $\cdot$ cm^{-3} $\cdot$ s^{-1}, respectively; however, the O(^{1}S) VER peak at a higher altitude of about 96 km on 18 December 2011 is only 338 photons $\cdot$ cm^{-3} $\cdot$ s^{-1}. The upper atmospheric VER values have been derived to transfer into the ground–based detected column intensities by our GBAII prototype. The calculated column integrated emission rates (IERs) of O_2(0-1) for 0° and 45° zenith angles are 1.48×10^7 and 1.91×10^7 photons $\cdot$ cm^{-2} $\cdot$ s^{-1}, respectively; the calculated column IERs of O(^{1}S) are 5.53×10^5 and 7.03×10^5 photons $\cdot$ cm^{-2} $\cdot$ s^{-1}, respectively. Correspondingly, the detected column IERs obtained by GBAII are 1.87×10^7 for O_2(0-1) and 6.57×10^5 photons $\cdot$ cm^{-2} $\cdot$ s^{-1} for O(^{1}S).

https://doi.org/10.1364/AO.99.099999

1. INTRODUCTION

Airglow is a low-light-level phenomenon caused by the solar electromagnetic radiation in the upper atmosphere of the Earth. When the direct or indirect solar radiation excites some atmospheric species to their higher energy level states, photons can be emitted by transitions from the excited states to the lower energy states due to instability. Because there is a longer lifetime at the excited states and the moving atmosphere species, the photons can run up to the balanced atmospheric emission, termed airglow, including dayglow and nightglow. In fact, as the airglow exists permanently in the upper atmosphere, it is very suitable for it to be used as a light source by passive remote sensing for measuring atmospheric wind and temperature. Although airglow is very difficult to detect due to its low light level intensity [1], the radiosonde, rocket, satellite measurement, and ground-based technologiesare developed to detect airglow [2]. With these advanced instruments, such important parameters in the upper atmosphere as wind vector, temperature, and volume emission rate (VER) can be obtained. Also, these excellent spatiotemporal resolution data sets provide support for research on gravity waves, ozone concentration [3], and other atmospheric compositions [4].

The theory and technology for detecting atmospheric temperature by using airglow emission were first proposed by the York University of Canada group in 1966 [5]. The Wind Imaging Interferometer (WINDII) [6], a wide-angle Michelson interferometer (MI) on NASA's upper atmospheric research satellite (UARS, 1991–2005), was a representative instrument that was able to measure the upper atmospheric (80–300 km) wind vector, temperature, and VER through multiple airglow emission lines. The high-resolution Doppler imager (HRDI) [7], another instrument on UARS, was also used to detect

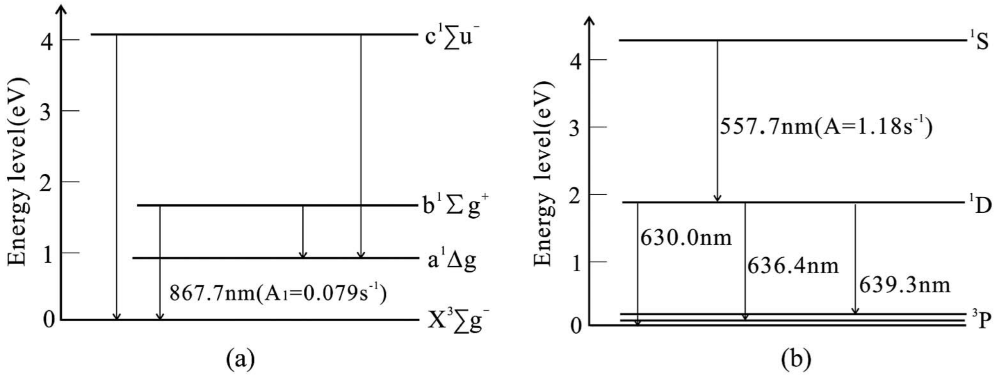

Fig. 1. Energy level scheme of O_2(0-1) and O(^{1}S) nightglows.

the low-middle atmospheric (10–120 km) wind field through Fabry–Perot interferometer (FPI) technology. The observation regions of WINDII and HRDI had a 40 km overlap in altitude, with the long-term observed results from them showing excellent agreement by two different applied technologies (MI and FPI) [8]. The VER of O_2(0 – 0) airglow at 94 km altitude observed by WINDII was about 4000–5000 photon $\cdot$ cm^{-3} $\cdot$ s^{-1} [2], while the VER peak of O(^{1}S) nightglow was 60–200 photon $\cdot$ cm^{-3} $\cdot$ s^{-1} at 90–97 km altitude (versus March 1993) [9]. The VER of O_2 (0-0) airglow at 94 km altitude was also obtained by HRDI [10]. The mesopause oxygen rotational temperature imager (MORTI), a ground-based instrument made to study the airglow, had been upgraded to measure VER O_2(0-1) and the vertically averaged temperature of the O_2(0-l) atmospheric band nightglow layer at 94 km altitude and OH (6-2) Meinel layer at 87 km [4]. The Spectral Airglow Temperature Imager (SATI), an improved version based on MORTI, was aimed at detecting rotational temperature and VER [11]. Sounding the atmosphere using broadband emission radiometry (SABER), another space-based instrument on the thermosphere ionosphere mesosphere energetics and dynamics (TIMED) satellite, obtained results from OH (6-2) airglow and nitric oxide VER (100–180 km) at 5.3 μm wavelength [12].

The airglow intensity as well as its VER has strong latitudinal, temporal, and local dependencies, and airglow detectors need to be distributed in different representative areas. Some local observations in northwest China (N34°, E108°) are presented in this paper. The ground-based airglow imaging interferometer (GBAII), which was proposed in earlier research by the authors, was capable of simultaneously measuring the wind vector and temperature at 90–100 km altitude [13,14]. GBAII, an integrated design of a wide-angle MI and a F-P filter, can employ both the "four intensity algorithms" [6] and "rotational line measurement temperature" methods [3]. A liquid-crystal on silicon (LCoS) is used as a mirror of the large air gap wide-angle MI [15] to be the static stepped device [16]. The nightglow sources of the O_2 atmospheric (0-1) band centered at 867.7 nm (867.8, 867.7, 867.3, 867.2, 866.2, 866.8, 866.6, 866.3, 866.2, 865.8, 865.7, 865.4, and 865.2 nm, 12 lines) and O(^{1}S) 557.7 nm (single line) are selected to detect the atmospheric wind vector and temperature by GBAII. The VERs of O_2(0-1) and O(^{1}S) nightglow are presented in subsequent sections of this paper.

The present paper is arranged as follows: Section 2 gives the simulation results on the VER of O_2(0–1) and O(^{1}S) nightglow based on the Barth mechanism; Section 3 describes the calculated nightglow integrated emission rate (IER) results for GBAII's geometry; Section 4 details the field experiments and the inversed nightglow IER results by using GBAII; Section 5 presents some discussions as well as a concluding summary.

2. SIMULATED NIGHTGLOW VER OF O_2(0-1) AND O(^{1}S)

For a certain atmospheric species, VER refers to the number of emitted phonons per second and volume from its higher energy level states to lower energy states. VER's unit is photons $\cdot$ cm^{-3} $\cdot$ s^{-1}, and its expression is

$$\mathrm{VER} = A \cdot [c], \tag{1}$$

where A denotes spontaneous radiation Einstein-A coefficient and $[c]$ denotes the atmospheric species concentration (number densities) like [O_2(0-1)] or [O(^{1}S)].

A. VER of O_2(0-1) Nightglow

Molecular oxygen O_2(0-1) 867.7 nm nightglow is the spectrum transfer of ($b^1\Sigma_g^+ \rightarrow X^3\Sigma_g^-$) shown in Fig. 1(a), where X is the ground state, b is the second excited state, Σ is the molecular excited state, g is the vibronic level symmetry, and u is the vibronic level antisymmetry. According to the Barth mechanism, the photochemical emission reaction involved in the O_2 atmospheric band spectrum can be described in the following two-step process [2]:

$$\mathrm{O} + \mathrm{O} + \mathrm{M}(\mathrm{O}_2 + \mathrm{N}_2) \rightarrow \mathrm{O}_2\left(c^1\sum\nolimits_u^-\right) + M, \tag{2}$$

$$\mathrm{O}_2\left(c^1\sum\nolimits_u^-\right) + \mathrm{O}_2 \rightarrow \mathrm{O}_2\left(b^1\sum\nolimits_g^+\right) + \mathrm{O}_2, \tag{3}$$

where the quenching of $O_2(b^1\sum_g^+)$ by the atmospheric O_2 and N_2 is included, and M is set to be equal to the molecules of [O_2] and [N_2]. For the two-step transfer of the Barth

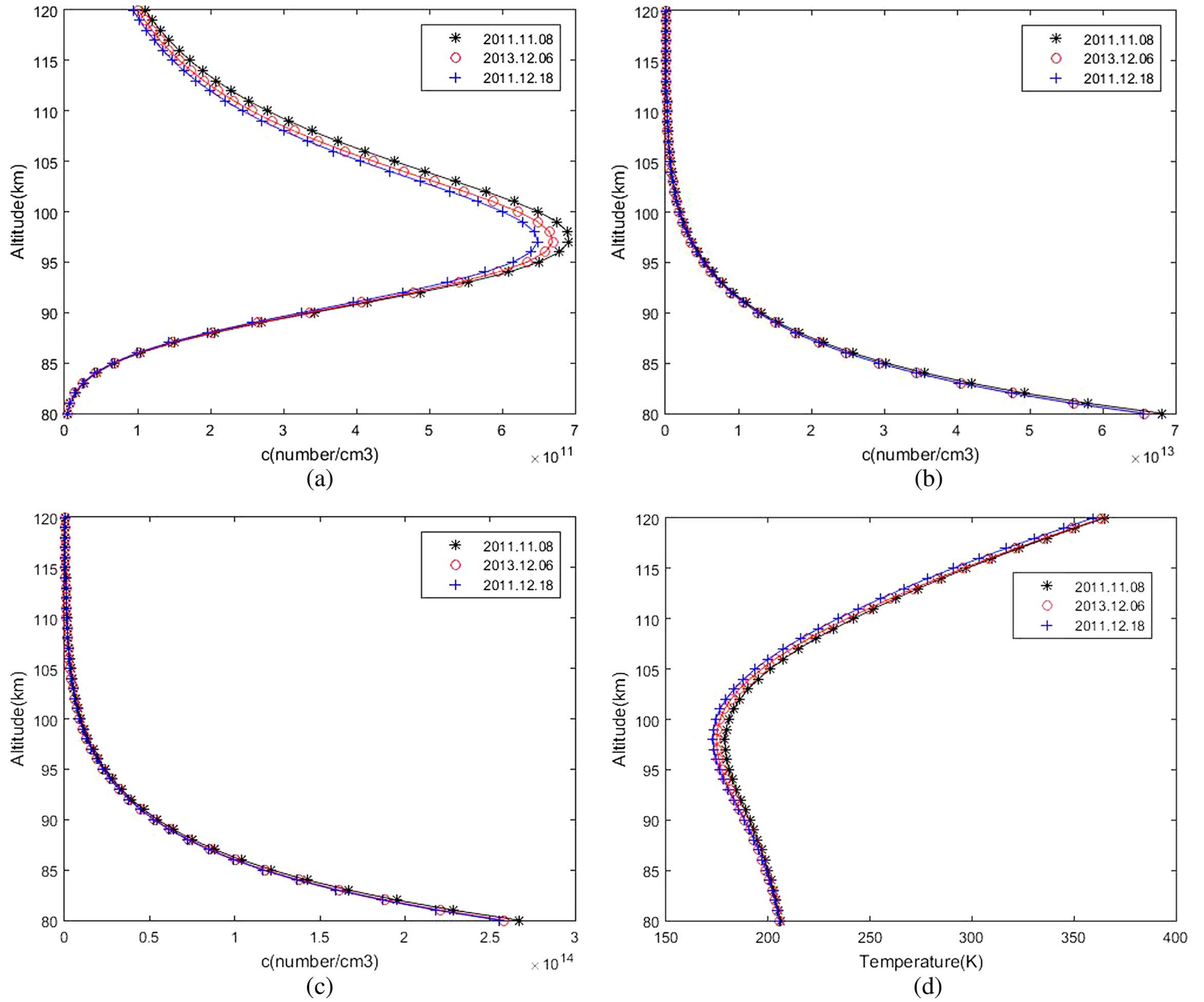

Fig. 2. Vertical concentration profiles mapping–altitude: (a) atoms' oxygen concentration, (b) molecule O_2 concentration, (c) molecule N_2 concentration, (d) upper atmospheric temperature.

mechanism, the VER for this process can be defined and evaluated by the following predecessor [17]:

$$\mathrm{VER}_{O_2(0\text{-}1)} = \frac{k_r A_1 [\mathrm{O}]^2([\mathrm{O}_2]+[\mathrm{N}_2])[\mathrm{O}_2]}{(A_2 + \mathrm{K}_2^{\mathrm{O}_2}\cdot[\mathrm{O}_2] + \mathrm{K}_2^{\mathrm{N}_2}\cdot[\mathrm{N}_2])\cdot(7.5[\mathrm{O}_2]+33[\mathrm{O}])}, \tag{4}$$

where k_r is the rate coefficient for the three-body recombination of the O atom; $k_r = 4.7\times10^{-33}(300/T)^2\ \mathrm{cm}^6\cdot\mathrm{s}^{-1}$. $\mathrm{K}_2^{\mathrm{O}_2} = 4\times10^{-17}\ \mathrm{cm}^3.\mathrm{s}^{-1}$ and $\mathrm{K}_2^{\mathrm{N}_2} = 2.2\times10^{-15}\ \mathrm{cm}^3.\mathrm{s}^{-1}$ are the rate coefficients for quenching by O_2 and N_2, respectively; A_1 and A_2 are the transition probabilities of (0-0) band and $O_2(b^1\sum_g^+)$ ($A_1 = 0.079\ \mathrm{s}^{-1}$ and $A_2 = 0.083\ \mathrm{s}^{-1}$), respectively; [O], $[O_2]$, and $[N_2]$ are, respectively, the number densities of atomic oxygen, molecular oxygen, and nitrogen.

The data of concentrations of atomic [O], molecular $[O_2]$, and $[N_2]$ as well as the upper atmospheric temperature profile of the Naval Research Laboratory Mass Spectrometer Incoherent Scatter (NRLMSISE-00) of the Community Coordinated Modeling Center (CCMC) are used in this paper [18]. According to the GBAII's parameters and the local observation time and place for the nightglows, for example, the experimental date (8 November 2011) and the geographical position of Xi'an (N34°13′23″, E 108°59′39″) in China, the discrete concentration or number densities can be obtained and are shown in Fig. 2. After bringing these number densities of [O], $[O_2]$, $[N_2]$ and corresponding atmospheric temperature into Eq. (4), a group of discrete VER values can be obtained, which are shown in Fig. 3(a). The VER peak values of VER were about 8111 and 8406 photons $\cdot\ \mathrm{cm}^{-3}\cdot\mathrm{s}^{-1}$ on 6 December 2013 and 8 November 2011, respectively, at 94 km altitude.

Because the VER profiles mapped to the altitude shown in Fig. 3 are Gaussian profiles, it is troublesome for the ground detected instrument, so we give a so-called "four-layer method" to fit the Gaussian profile. The aim is to transform the integral

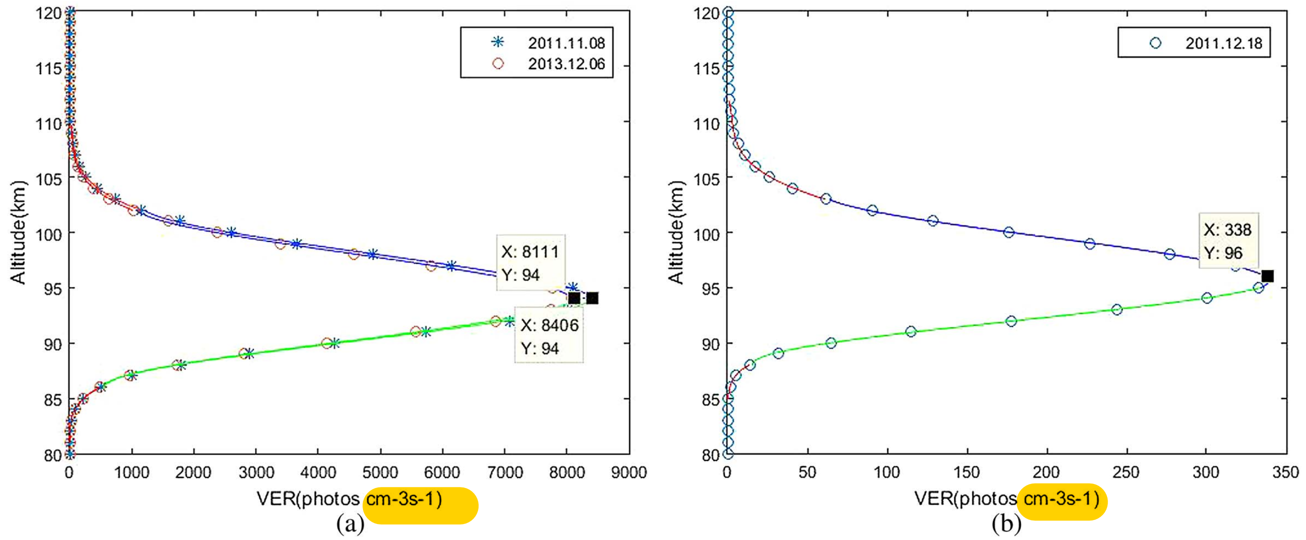

Fig. 3. Nightglow VER profile mapping–altitude: (a) O2(0–1) 867.7 nm nightglow, (b) $O(^1S)$ 557.7 nm nightglow.

Table 1. Fitting Coefficients versus Eq. (5) of O_2(0-1) VER Profile for Two Dates

	8 November 2011				6 December 2013			
Altitude	a_1	a_2	a_3	a_4	a_1	a_2	a_3	a_4
$81 < h < 86$ km	5.4145	-1.3236×10^3	1.0785×10^5	-2.9292×10^6	5.2482	-1.2830×10^3	1.0454×10^5	-2.8394×10^6
$86 < h < 94$ km	−28.219	7.6283×10^3	-6.8593×10^5	2.0521×10^6	−27.786	7.5089×10^3	-6.7502×10^5	2.0190×10^7
$94 < h < 102$ km	22.410	-6.5978×10^3	6.4622×10^5	-2.1052×10^7	21.747e	-6.3960×10^3	6.2583×10^5	-2.0367×10^7
$102 < h < 110$ km	−3.6638	1.1919×10^3	-1.2928×10^5	4.6743×10^6	−3.4401	1.1182×10^3	-1.2117×10^5	4.3773×10^6

VER value conveniently along the line of sight for the column IER detected by the ground-based CCD detector. In later Section 3.B, a local continuous series of powers of the VER profile needs to be fitted with the results shown in Fig. 3(a). Of course, at the NRLMSISE window condition, our Xi'an local time 2:00 am and location of longitude and latitude (N34°, E108°) are selected as perfectly as possible to match GBAII's observation conditions. The VER profile is a function of altitude h and is expressed as

$$\mathrm{VER}(h) = a_1 h^3 + a_2 h^2 + a_3 h + a_4, \tag{5}$$

where a_1, a_2, a_3, and a_4 are different coefficients. For the best fitting degree, h is divided into four regions, i.e., 81–86 km, 86–94 km, 94–102 km, and 102–110 km O_2(0-1) nightglows shown in Fig. 3(a). The corresponding coefficients of a_1, a_2, a_3, and a_4 for two days are shown in Table 1. The fitting degree is 99.0% according to the least-squares method.

B. VER of $O(^1S)$ Nightglow

According to the Barth mechanisms, the atomic oxygen $O(^1S)$557.7 nm nightglow emission transition shown in Fig. 1(b) can be expressed as the transition of $O(^1S) \rightarrow O(^1D)$. In order to calculate the VER of $O(^1S)$, the $O(^1S)$ concentration must be known for Eq. (1). By following three photochemical reaction actions, the concentration can be obtained as follows:

$$\mathrm{O} + \mathrm{O} + M \xrightarrow{k_1} \mathrm{O}_2^* + M, \tag{6}$$

$$\mathrm{O}_2^* + \mathrm{O} \xrightarrow{\delta k_{\mathrm{O}}} \mathrm{O}(^1S) + \mathrm{O}_2. \tag{7}$$

For a balanced atmosphere, generation rate is equal to the consumption rate, and thus there is the following equilibrium equation:

$$\mathrm{O}(^1S) \xrightarrow{A_{577.7}} \mathrm{O}(^1D) + h\nu(557.7\ \mathrm{nm}). \tag{8}$$

The VER of $O(^1S)$ can be written as [18]

$$\mathrm{VER}_{\mathrm{O}(^1S)} = \frac{A_{557.7\,\mathrm{nm}} k_1 [\mathrm{O}]^3 [M]}{(A(^1S) + k_2[\mathrm{O}_2])(C_0 + C_1[\mathrm{O}] + C_2[\mathrm{O}_2])}, \tag{9}$$

where $C_0 = A(\mathrm{O}_2^*)/\beta\delta k_{\mathrm{O}}$, $C_1 = 1/\beta\delta$, $C_2 = (k_{\mathrm{O}_2} + R k_{\mathrm{N}_2})/\beta\delta k_{\mathrm{O}}$, $R = [\mathrm{N}_2]/[\mathrm{O}_2]$, and $M = [\mathrm{O}_2] + [\mathrm{N}_2]$. The values of the parameters are $k_1 = 4.7 \times 10^{-33}(300/T)^2\ \mathrm{cm}^6\,\mathrm{s}^{-1}$, $k_2 = 4.0 \times 10^{-12} \exp(-867/T)\ \mathrm{cm}^3\,\mathrm{s}^{-1}$, $A_{557.7\,\mathrm{nm}} = 1.18\ \mathrm{s}^{-1}$, $A(^1S) = 1.35\ \mathrm{s}^{-1}$, $C_0 = 0$, $C_1 = 211$, and $C_2 = 15$ [18], respectively. Similarly, the discrete and fitted VER values of $O(^1S)$ 557.7 nm nightglow can be obtained [see Fig. 3(b)] after substituting the number densities of atomic [O] and molecular $[O_2]$ into Eq. (10) from NRLMSISE-00 [19]. The peak value of the VER was about 338.3 photons $\cdot\ \mathrm{cm}^{-3} \cdot \mathrm{s}^{-1}$ on 18 December 2011 at 96 km altitude. As O_2(0–1) nightglow, we define four

Table 2. Nightglow's Transmittance versus the Wavelength and the Zenith Angle

Wavelength (nm)	Transmittance (0° zenith angle)	Transmittance (45° zenith angle)	Selected Parameters from MODTRAN Model	Date
867.7	0.670	0.567	Urban visibility of 10 km, ground temperature of 278 K	8 Nov. 2011
867.7	0.671	0.560	Urban visibility of 10 km, ground temperature of 270 K	6 Dec. 2013
867.7	0.833	0.758	Rural visibility of 23 km, ground temperature of 278 K	18 Apr. 2018
557.7	0.658	0.551	Rural visibility of 23 km, ground temperature of 273 K	18 Dec. 2011

homologous altitude h regions, and the corresponding VER expressions are directly obtained by MATLAB as follows. (The recent corresponding MODTRAN data is only updated by the deadline on 17 April 2017, so we only give one simulation equation). The fitting degree is 98.8% according to the least-squares method. The VER expressions are

$$\begin{cases} \mathrm{VER}_1(h) = 0.5023h^3 - 1.2845\times10^2h^2 + 1.0950\times10^4h - 3.1118\times10^5 & (85 \le h < 88\ \mathrm{km}), \\ \mathrm{VER}_2(h) = -1.3727h^3 + 3.7895\times10^2h^2 - 3.4809\times10^4h + 1.0640\times10^6 & (88 \le h < 95\ \mathrm{km}), \\ \mathrm{VER}_3(h) = 1.0916h^3 - 3.2613\times10^2h^2 + 3.2426\times10^4h - 1.0727\times10^6 & (95 \le h < 103\ \mathrm{km}), \\ \mathrm{VER}_4(h) = -0.1410h^3 + 4.6622\times10^1h^2 - 5.1381\times10^3h + 1.8878\times10^5 & (103 \le h \le 112\ \mathrm{km}), \end{cases} \tag{10}$$

3. CALCULATED NIGHTGLOW IER FOR GBAII

A. Nightglow Transmittance

When the nightglow emission at 80–120 km altitude arrives at our ground-based GBAII detector after penetrating the atmospheric layer below, its IER will be reduced due to the atmospheric scattering and absorption. The atmospheric molecules' absorption and scattering at 867.7 nm and 557.7 nm are due to water vapor, carbon dioxide, and aerosols. In fact, the molecules' absorption and scattering can be ignored [20], and the atmospheric attenuation factor is considered more in the atmosphere below 10 km altitude, so the scattering may be considered to be affected by the aerosol influence for the dusty climates of Northwest China where GBAII's experiment is performed.

Although the wavelength 867.7 nm is just at the atmospheric window, the atmospheric transmittance must be calculated when the nightglow enters the GBAII's detector. The MODTRAN (moderate resolution atmospheric transmission) [21] is used as a reference for the nightglow transmittance. Appropriate parameters for the GBAII are selected as input for MODTRAN. We set the "Atmosphere Model" parameter to be mid-latitude summer and winter, the "Ground Temperature" parameter to be the actual experiment temperature, and the "Aerosol Models" parameter to be rural and urban. According to the GBAII's different observation place, the "Visibility" parameter was 23 km and 10 km, and the "Sensor Zenith" was 180° and 135°. The nightglow transmittance results are listed in Table 2.

B. Calculation Nightglow IER for GBAII

As a ground-based station device, the GBAII is able to accept the full photon column of the nightglow intensity profile at 80–120 km as shown in Fig. 3. The nightglow emission is gathered together by the GBAII detector, which has a field of view (FOV) incident angle of 6°, and the slanting optical path nightglow for the 45° zenith angle of incident light [13,14] is shown as the green region in Fig. 4. Thus, the nightglow IER detected by GBAII's CCD detector can receive the nightglow photons from the ground to 120 km altitude as follows:

$$\mathrm{IER}_C = \int_{r_1}^{r_2}\int_{\theta=0^\circ}^{\theta=6^\circ}\int_{\varphi=0}^{2\pi}\frac{\mathrm{VER}}{4\pi r^2}\tau\cdot r^2\sin\theta\,\mathrm{d}r\mathrm{d}\theta\mathrm{d}\varphi, \tag{11}$$

where I_{IER} is the calculated number of photons accepted by the GBAII's CCD per area, τ is the atmospheric transmittance, $\mathrm{VER}(h)$ is as mentioned earlier in Eq. (5), r is the slanting optical path from the GBAII to the nightglow species, and $r_1 = 80$ km, $r_2 = 120$ km, and $\mathrm{VER}(h)$ are the different expressions followed by Eq. (5) versus Table 1 and Eq. (11). There is the following relation between r and h (see Fig. 4):

$$(R_0 + h)^2 = r^2 + R_0^2 - 2rR_0\cos(\pi - \theta_0 - \theta), \tag{12}$$

where R denotes the Earth's radius, h denotes altitude from 80 to 120 km, $R_0 = R + h$, θ_0 denotes the GBAII's zenith angle of incidence, and θ denotes the GBAII's FOV. As $R_0 \gg h$, Eq. (12) can be simplified to

$$h = r\cos(\theta_0 + \theta). \tag{13}$$

According to Eqs. (5), (11), and (13), the IER_C can be

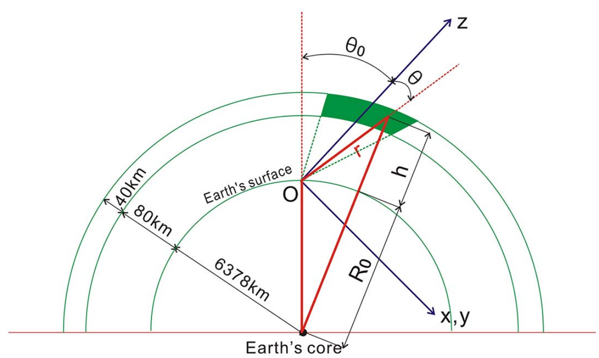

Fig. 4. Airglow contribution height for the GBAII's measurement geometry.

Table 3. Nightglow IER Results for GBAII[a,b]

Observation Date	Nightglow	Calculated IER_C (0° zenith angle)	Calculated IER_C (45° zenith angle)	Detected IER_D (45° zenith angle)	Error
8 Nov. 2011	$O_2(0–1)$	1.48×10^7	1.91×10^7	1.87×10^7	2.1%
6 Dec. 2013	$O_2(0–1)$	1.42×10^7	1.79×10^7	1.27×10^7	29.0%
18 Apr. 2018	$O_2(0–1)$	No data	No data	1.29×10^7	
18 Dec. 2011	$O(^1S)$	5.53×10^5	7.03×10^5	6.57×10^5	6.5%
18 Apr. 2018	$O(^1S)$	No data	No data	1.347×10^6	

[a]Unit: photons $\cdot$ $cm^{-2} \cdot s^{-1}$.
[b]Remarks: "No data" is because MODTRAN data is only updated to 17 April 2017.

$$IER_C = \int_{\theta=0}^{6^\circ}\int_{r_1}^{r_2}\int_{\varphi=0}^{2\pi}\frac{VER[r\cos(\theta_0+\theta)]\cdot 10^6}{4\pi r^2}\cdot\tau\cdot r^2\sin\theta d\varphi dr d\theta. \quad (14)$$

Bringing Eq. (10) into Eq. (14), the nightglow IER_c is

$$IER_C = \frac{\tau}{2}\cdot 10^5\cdot\left(\frac{a_1}{4}h^4+\frac{a_2}{3}h^3+\frac{a_3}{2}h^2+a_4h\right)\Bigg|_{80}^{120}\cdot\left[-\cos\theta_0\ln\frac{\cos(\theta_0+6)}{\cos\theta_0}-6\sin\theta_0\right], \quad (15)$$

where the unit of IER_C is photons $\cdot$ $cm^{-2}\cdot s^{-1}$, the unit of h is denoted by kilometers (km), and the factor of 10^5 is the united unit result from. Using t, τ, and a_1–a_4 for each experiment into Eq. (16), the calculated IER of nightglow can be obtained. For example, for $O_2(0–1)$ 867.7 nm nightglow, let $\tau =$ 0.658 and 0.551 (see Table 2), and bringing the VER (h) functions in Eq. (5) versus Table 1 and Eq. (10) into Eq. (15), with the corresponding atmospheric transmittance listed in Table 2, the nightglow IER can be calculated. The results are 1.91×10^7(photons $\cdot$ $cm^{-2}\cdot s^{-1}$) and 1.48×10^7(photons $\cdot$ $cm^{-2}\cdot s^{-1}$) when $\theta_0 = 45°$ and $\theta_0 = 0°$, respectively. For $O(^1S)$ 557.7 nm nightglow, when $\tau = 0.658$ and 0.551 (see Table 2), its calculated intensity is 7.03×10^5(photons $\cdot$ $cm^{-2}\cdot s^{-1}$) for $\theta_0 = 45°$, and the calculated IER is 5.53×10^5(photons $\cdot$ $cm^{-2}\cdot s^{-1}$) for $\theta_0 = 0°$. [For the other data, see Columns 3 and 4 in Table 3; all detected time is 200 s and 300 s for $O_2(0–1)$ and $O(^1S)$, respectively].

4. DETECTED NIGHTGLOW IER BY GBAII

A. Detected Nightglow IER Principle

The key components of the GBAII prototype made by our group contain a wide-angle MI with a large air gap and a narrowband FPI [16]. The GBAII is used to measure the upper atmospheric (80–120 km) wind velocity, temperature, VER, pressure, and gravitational wave. Some results are satisfactory [13,14]. The nightglow VER can also be inverted from the intensity of the imaging interference fringes of the GBAII, which can be written as

$$I(\Delta) = I_0[1+\exp(QT\Delta^2)\cos(2\pi\sigma_0\Delta)], \quad (16)$$

where $Q = 1.82\times 10^6/m\lambda_0^2$, λ_0 is wavelength at zero wind speed ($\lambda_0 = 867.7$ nm, or 557.7 nm), Δ is MI's total optical path difference (OPD), I_0 is the max intensity of the interference fringes, and m is the atomic mass. When the quantum numbers of the O_2 molecular vibrational-rotational spectrum vary, the max intensity I_0 in Eq. (16) is different, as it has been modulated by the FPI of the GBAII. The four-intensity-algorithm technique [6] requires the OPD Δ in Eq. (16) to be divided into two parts, i.e., fixed OPD Δ_0 and stepped OPD Δ' ($\Delta = \Delta_0 + \Delta'(\Delta_0 \gg \Delta')$). For the GBAII, $\Delta_0 =$ 7.495 cm, and the stepped OPD $\Delta' = 0, \lambda_0/4, 2\lambda_0/4$, and $3\lambda_0/4$ ($\lambda_0 = 867.7$ nm or 557.7 nm), respectively. Under the combined influence of the MI and FPI of the GBAII, the group intensity for the quantum number j is

$$\begin{cases} I_{1(j)} = I_{0(j)}[1+UV\cos\phi_{(j)}],\\ I_{2(j)} = I_{0(j)}[1-UV\sin\phi_{(j)}],\\ I_{3(j)} = I_{0(j)}[1-UV\cos\phi_{(j)}],\\ I_{4(j)} = I_{0(j)}[1+UV\sin\phi_{(j)}], \end{cases} \quad (17)$$

where U and V are the resolutions of the GBAII instrument and the interference fringe. With the four fringe intensities worked out, the max intensity of $I_{0(j)}$, which is just related to the nightglow VER, can be obtained through Eq. (17) as

$$I_{0(j)} = [I_{1(j)}+I_{3(j)}]/2 = [I_{2(j)}+I_{4(j)}]/2, \quad (18)$$

where the quantum number j corresponds to a rotational line. It should be pointed out that, for the single atom airglow of $O(^1S)$, the intensity I_0 only needs one fringe to invert the average IER, and the quantum number j is not a requisite. The intensities in Eq. (18) can be read by the GBAII's CCD, whose imaging interference fringes are shown through the experiments in a later section. The operated intensity of Eq. (17) is just replaced by the average IER for one given fringe.

B. Experiments by GBAII

A series of urban and rural experiments were carried out with GBAII in northwest China. Some of the GBAII's pictures are selected to calculate VER. Four nightglow images of interference fringes for different dates and geographical positions are shown in Figs. 5(a)–5(d), where the white dots are stars or cosmic rays.

For the $O_2(0–1)$ 867.7 nm nightglow, the pictures of imaging interference fringes taken on 8 November 2011 and 6 December 2013 before daybreak at the urban area Xi'an inChina, which is situated at N34°13′23″ and E108°59′39″, 457 m above sea level, are selected. One of the four stepped imaging interferometer fringes has been shot and is shown in Figs. 5(a) and 5(b). The CCD pixels are 512 × 512 (2 × 2 pixels for a bin), and the peak quantum efficiency is 0.38. The exposure time of each picture is 200 s.

Similarly, for the O_2(0-1) 867.7 nm nightglow, the pictures of the imaging interference fringes shown in Fig. 5(c) were obtained on 18 April 2018 before daybreak at the rural area of the

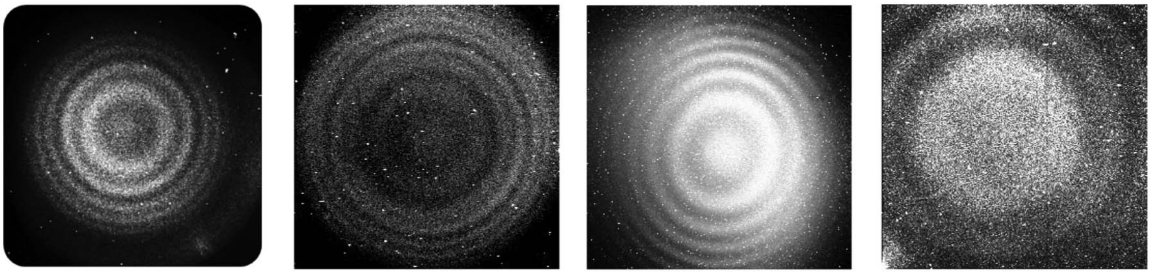

(a) (b) (c) (d)

Fig. 5. Imaging interference fringe of O_2(0-1) 867.7 and O(^{1}S) nightglow observed by the GBAII (a) O2(0-1) at Xi'an University Qujiang campus (urban), N34°13′23″, E 108°59′39″, 8 November 2011; (b) O2(0-1) at Xi'an University Qujiang campus (urban), N34°13′23″, E 108°59′ 39″, 6 December 2013; (c) O2(0-1) at Ren zong miao (rural), N34°19′56′′, E109°16′53′′, 18 April 2018; (d) O(1S) at Ren zong miao (rural), N34° 19′56′′, E109°16′53′′, 18 December 2011.

Zhuque Forest Park in China, which is located at N33°50′1″ and E108°30′50″, 1200 m above sea level. All the GBAII's CCD shooting conditions and parameters in Fig. 5(c) are the same as those in Fig. 5(a). The exposure time of each picture is 200 s.

For the O(^{1}S) 557.7 nm nightglow, the imaging interference fringes in Fig. 5(d) were obtained on 18 December 2011 before daybreak at the rural mountaintop of Ren zong Miao of Lin tong, which is situated at N34°19′56′′ and E109°16′53′′, 1302 m above sea level. All of the GBAII's CCD shot conditions and parameters in Fig. 5(d) are the same as those in Fig. 5(a), except the exposure time of 300 s and altitude of 1302 m. The exposure time of each picture is 300 s.

C. Retrieved Nightglow IER for GBAII

With the nightglow pictures shown in Figs. 5(a)–5(d) obtained, the following expression is used to calculate the detected nightglow IER_D so as to derive the VER value:

$$\mathrm{IER}_D = (N_s - N_d) \cdot \frac{1}{0.004^2} \cdot \frac{C_{\mathrm{ADV}}}{\eta} \cdot \frac{1}{\xi} \cdot \frac{1}{\tau_{\mathrm{sys}}} \cdot \frac{1}{t}, \tag{19}$$

where N_s is the electron counting read from one imaging interference fringe on the GBAII's CCD, which should be the total count rate in counts, N_d is the dark current, t is observation time [t is 200s for O_2(0–1), 300 s for O^1(S)], C_{ADV} is the CCD's digital-to-analog conversion efficiency, η is the CCD's quantum efficiency, ξ is the P(0–1) branch pair of the lines' carrier value of the O_2(0–1) band emission [22], and τ_{sys} is the GBAII's transmittance. The value of 0.004 cm^2 is the united conversion of CCD pixel size (20 micron) to centimeters.

According to the factory parameters $C_{\mathrm{ADV}} = 2$ and $\eta = 0.38$ (for 867.7 nm wavelength) and $\eta = 0.55$ (for 557.7 nm wavelength), the parameters of N_d and τ_{sys} are detected in lab as $N_d = 100$, $\tau_{\mathrm{sys}} = 0.18$, $\xi = 7.5\%$. By the software "Image J," one of the imaging interference fringes is used to read the electron count. Bringing these parameters and the count into Eq. (17), the nightglow IER of O_2(0-1)867.7 nm can be obtained, and it is 1.29×10^7(photons $\cdot\ \mathrm{cm}^{-2} \cdot \mathrm{s}^{-1}$) (test date: 18 April 2018). Other calculated and experimental results of the IER are shown in the fifth column of Table 3.

D. Error and Analysis

According to the calculated IER_C and detected IER_D in Eqs. (15) and (18), the relative errors are shown in the sixth column of Table 3.

Because our GBAII is a ground-based device that measures the integral of the upper atmospheric VER profile along the line of sight, the number of photons emitted from a centimeter squared column along that line of sight every second. The minimum relative error of the VER of O_2(0-1) measured by the GBAII is 2.1%, the maximum error is 29.0%, and the error of the VER of O(^{1}S) is 6.5% as shown in Table 3. Although the error for nitric oxide (NO) VER observed from the space-based SABER is 15% [12] and O_2 (0-0) VER error measured by HRDI is 10% [10], the GBAII has accuracy limitations compared to other instruments. However, with mass data and suitable analysis this limitation may be reduced and the GBAII's accuracy may be improved. We need more data to establish the daily variability in order to investigate the seasonal variability.

The relative errors are defined from comparisons with the simulations using NRLMSISE data. However, those are just differences with this model simulation, and it should be noted that they may have errors of every different nature (temperature, abundances, and pressures). Because the VERs are simulated and calculated based on the models of NRLMSISE-00 and MODTRAN in this paper, the model of "atmospheric visibility" only has the selected alternatives of 23 km or 10 k" to reach the parameters in Eq. (5) and the MODTRAN model. However, our local detected data are in northwest China, which has dusty climate conditions. The geographical position in the present study is in northwest China where sandstorms occur more frequently, although the all experiments carried out by the GBAII were selected to detect after rain. In fact, the actual atmospheric visibility cannot achieve the model's atmospheric visibility. Additionally, different aerosol scenarios should be considered, since the atmospheric transmittance is a factor of the column IER. We think this is one reason that may lead to the error between the calculated and detected IERs of the nightglows.

5. CONCLUSIONS

In order to obtain the upper atmospheric VER at 80–120 km altitude in northwest China, this paper studied the VER of

O_2(0-1) and O(^{1}S) species nightglow based on the Barth mechanism, with the main conclusions being as follows.

The nightglow VER profile of O_2(0-1) has been simulated and the peak values of VER at 94 km altitude on experimental dates 6 December 2013 and 8 November 2011 are 8111 and 8406 photons $\cdot$ cm^{-3} $\cdot$ s^{-1}, respectively. The nightglow emission will be attenuated by the atmosphere, and its simulated transmittances of O_2(0-1) for 8 November 2011 are 0.670 (0.671) and 0.567 (0.560) when the zenith angles are 0° and 45°, respectively. After the nightglow VER is changed into the IER, the theoretical calculation nightglow IER_C values of O_2(0–1) for 0° and 45° zenith angles, respectively, are 1.48×10^7 and 1.91×10^7 photons $\cdot$ cm^{-2} $\cdot$ s^{-1}. The detected IER_D values of O_2(0-1) nightglow for 45° zenith angle by the GBAII on 8 November 2011 and 6 December 2013 are 1.87×10^7 and 1.27×10^7 photons $\cdot$ cm^{-2} $\cdot$ s^{-1}, respectively.

The nightglow VER profile of O(^{1}S) has been simulated and the peak value of VER is 338 photons $\cdot$ cm^{-2} $\cdot$ s^{-1} at 96 km. The nightglow emission is going to be attenuated by the atmosphere, and the simulated transmittances of O(^{1}S) for 0° and 45° zenith angles, respectively, are 0.658 and 0.551 on 18 December 2011. After the nightglow VER is changed into the IER, the theoretical nightglow IER_C values of O(^{1}S), respectively, are 5.53×10^5 and 7.03×10^5 photons $\cdot$ cm^{-2} $\cdot$ s^{-1} for 0° and 45° zenith angles. The IER_D value of O(^{1}S) nightglow detected by GBAII is 6.57×10^5 photons $\cdot$ cm^{-2} $\cdot$ s^{-1}.

Funding. National Natural Science Foundation of China (NSFC) (61675165); Natural Science Foundation of Shaanxi Province (2016JM1011); National Instrument Development Special Program (2013YQ030651); Characteristic Fund of Xi'an University of Technology (2015TS012); Open Research Fund of Key Laboratory of Spectral Imaging Technology, Chinese Academy of Sciences (LSIT201714D).

REFERENCES

1. Y. H. Tang, X. G. Cao, H. C. Liu, G. G. Shepherd, S. L. Liu, H. Y. Gao, X. S. Yang, Y. Wu, and S. W. Wang, "Partially light-controlled imager based on liquid crystal plate and image intensifier for aurora and airglow measurement," Appl. Opt. **51**, 1968–1975 (2012).
2. G. G. Shepherd, G. Thuillier, Y. M. Cho, M. L. Duboin, W. F. J. Evans, W. A. Gault, C. Hersom, D. J. W. Kendall, C. Lathuillère, R. P. Lowe, I. C. McDade, Y. J. Rochon, M. G. Shepherd, B. H. Solheim, D. Y. Wang, and W. E. Ward, "The wind imaging interferometer(WINDII) on the upper atmosphere research satellite: a 20 year perspective," Rev. Geophys. **50**, RG2007 (2012).
3. R. H. Wiens, S. P. Zhang, R. N. Peterson, and G. G. Shepherd, "MORTI: a menopause oxygen rotational temperature imager," Planet. Space Sci. **39**, 1363–1375 (1991).
4. R. H. Wiens, A. Moise, S. Brown, S. Sargoytchev, R. N. Peterson, G. G. Shepherd, M. J. Lopez-Gonzalez, J. J. Lopez-Moreno, and R. Rodrigo, "SATI: a spectral airglow temperature imager," Adv. Space Res. **19**, 677–680 (1997).
5. R. L. Hilliard and G. G. Shepherd, "Upper atmospheric temperatures from Doppler line widths," Planet. Space Sci. **14**, 383–406 (1966).
6. G. G. Shepherd, G. Thuillier, and W. A. Gault, "WINDI I, the wind imaging interferometer on the upper atmosphere research satellite," J. Geophys. Res. **98**, 10725–10750 (1993).
7. P. B. Hays, V. J. Abreu, and M. E. Dobbs, "The high-resolution Doppler imager on the upper atmosphere research satellite," J. Geophys. Res. **98**, 10713–10723 (1993).
8. C. McLandress, G. G. Shepherd, B. H. Solheim, M. D. Burrage, P. B. Hays, and W. R. Skinner, "Combined mesosphere/thermosphere winds using WINDII and HRDI data from the upper atmosphere research satellite," J. Geophys. Res. **101**, 10441–10453 (1996).
9. R. H. Wiens, M. J. Taylor, S. P. Zhang, and G. G. Shepherd, "Coupled longitudinal and tidal variations of equatorial nightglow O(1S) zenith emission rates from WIND11 and Christmas Island data," Adv. Space Res. **24**, 1577–1582 (1999).
10. D. A. Ortland, P. B. Hays, and W. R. Skinner, an J. H. Yee, "Remote sensing of mesospheric temperature and $O_2(^1\Sigma)$ band volume emission rates with the high-resolution Doppler imager," J. Geophys. Res. **103**, 1821–1835 (1998).
11. M. J. Lopez-Gonzalez, M. Garcıa-Comas, E. Rodrıgueza, M. Lopez-Puertas, M. G. Shepherd, G. G. Shepherd, S. Sargoytchev, V. M. Aushev, S. M. Smithd, M. G. Mlynczak, J. M. Russell, S. Brown, Y. M. Cho, and R. H. Wiens, "Ground-based mesospheric temperatures at mid-latitude derived from O_2 and OH airglow SATI data: comparison with SABER measurements," J. Atmos. Sol. Terr. Phys. **69**, 2379–2390 (2007).
12. J. Oberheide, M. G. Mlynczak, C. N. Mosso, B. M. Schroeder, B. Funke, and A. Maute, "Impact of tropospheric tides on the nitric oxide 5.3 μm infrared cooling of the low-latitude thermosphere during solar minimum conditions," J. Geophys. Res. **118**, 7283–7293 (2013).
13. H. Y. Gao, Y. H. Tang, D. X. Hua, H. C. Liu, X. G. Cao, X. D. Duan, Q. J. Jia, O. Y. Qu, and Y. Wu, "Ground based airglow imaging interferometer part 1: instrument and observation," Appl. Opt. **52**, 8650–8660 (2013).
14. Y. H. Tang, X. D. Duan, H. Y. Gao, O. Y. Qu, Q. J. Jia, X. G. Cao, S. N. Wei, and R. Yang, "Ground based airglow imaging interferometer part 2: forward model and inverse method," Appl. Opt. **53**, 2272–2282 (2014).
15. H. Y. Gao, D. X. Hua, Y. H. Tang, X. G. Cao, H. C. Liu, and W. L. Jia, "Wide-angle Michelson interferometer based on LCoS," Opt. Commun. **292**, 36–41 (2013).
16. H. Y. Gao, Y. H. Tang, D. X. Hua, and H. C. Liu, "Study on the wide-angle Michelson interferometer with large air gap," Appl. Opt. **50**, 5655–5661 (2011).
17. F. Vargas, G. Swenson, A. Liu, and D. Gobbi, "O(^{1}S), OH, and O_2(b) airglow layer perturbations due to AGWs and their implied effects on the atmosphere," J. Geophys. Res. **112**, D14102 (2007).
18. E. S. David and E. S. William, "A comparison of measurements of the oxygen nightglow and atomic oxygen in the lower thermosphere," Planet. Space Sci. **39**, 627–639 (1991).
19. "Community Coordinated Modeling Center," https://ccmc.gsfc.nasa.gov/modelweb/models/nrlmsise00.php#opennewwindow.
20. Y. H. Tang, R. Yang, H. Y. Gao, F. T. Zhai, Y. Yu, and J. Cui, "Improving the atmospheric wind speed measured accuracy by the ground-based airglow imaging interferometer," Proc. SPIE **10256**, 102563C (2017).
21. http://modtran.spectral.com/modtran_home.
22. R. L. Gattinger, *Synthetic Spectrum of O2 Atmospheric System, Herzberg Institute of Astrophysics Software* (1984).

Queries

1. AU: Edit to title OK?

2. AU: Please check if there is missing text at the end of this sentence after “from”:“where the unit of IERC is photons•cm−2•s−1, the unit of *h* is denoted by kilometers (km), and the factor of 105 is the united unit result from.”

3. AU: Please check the edit made to the following sentence: “ξ is the P(0-1) branch pair of the lines carrier value of the O2(0-1) band emission [22].”

4. AU: Please check if there is missing text at the end of this sentence: “Because our GBAII is a ground-based device that measures the integral of the upper atmospheric VER profile along the line of sight, the number of photons emitted from a centimeter squared
521 column along that line of sight every second.”

5. AU: Please define “SABER” in this sentence: “Although the error for nitric oxide (NO) VER observed from the space-based SABER is 15%”

6. AU: The funding information for this article has been generated using the information you provided to OSA at the time of article submission. Please check it carefully. If any information needs to be corrected or added, please provide the full name of the funding
522 organization/institution as provided in the CrossRef Open Funder Registry (https://search.crossref.org/funding).